# Resonant Mixing-Dynamic Nuclear Polarization

Yifan Quan,[1] Yifu Ouyang,[1] Michael Mardini,[1] Ravi Shankar Palani,[1] Daniel Banks,[2] James Kempf,[2] W. Tom Wenckebach,[3,4] and Robert G. Griffin[1, 1]

[1] *Francis Bitter Magnet Laboratory and Department of Chemistry, Massachusetts Institute of Technology, Cambridge, Massachusetts 02139, United States*
[2] *Bruker Biospin, 15 Fortune Drive, Billerica, MA 01821, United States*
[3] *Paul Scherrer Institute, 5232 Villigen PSI, Switzerland*
[4] *National High Magnetic Field Laboratory, University of Florida, Gainesville, FL 32310, United States*

(Dated: January 19, 2023)

We propose a new mechanism for dynamic nuclear polarization that is different from the well-known Overhauser effect, solid effect, cross effect and thermal mixing processes. In particular, we discovered that the evolution of the density matrix with the simple Hamiltonian of a coupled electron-nuclear spin pair with weak microwave irradiation yields a nuclear polarization enhancement when irradiating near the electron Larmor frequency. We denote the mechanism as *Resonant Mixing (RM)*. We believe that this mechanism is responsible for the observed dispersive shaped DNP field profile for trityl samples near the electron paramagnetic resonance center. This new effect is due to mixing of states by the microwave field together with the electron-nuclear coupling, and involves the same interactions as the SE. However, the SE is optimal when the microwave field is off-resonance, whereas RM is optimal when the microwave field is on-resonance.

TOC graphic

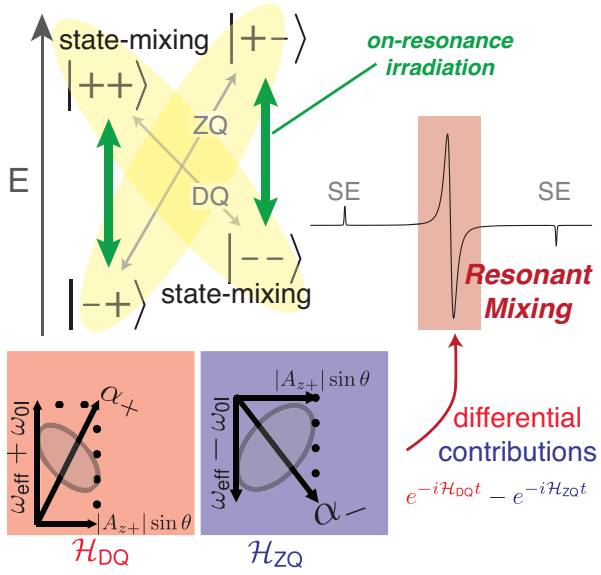


Dynamic nuclear polarization (DNP) is used to enhance the polarization of nuclear spins by transferring polarization from unpaired electrons via microwave irradiation [1]. Accordingly, in the last two decades high frequency DNP has evolved as one of the most powerful and widely applicable techniques to mitigate the chronic issue of sensitivity in nuclear magnetic resonance (NMR) spectroscopy [2, 3]. In particular, in the recent past microwave driven DNP has been successfully applied to protein structural studies [4-11], to a variety of problems in materials science [12-14], and to applications of magnetic resonance imaging (MRI) using dissolution-DNP [15, 16]. Descriptions of the theoretical background of DNP can be found in review articles and one monograph[2, 3, 17-22].

The collection of the four fundamental mechanisms used in continuous wave (CW) DNP experiments are the Overhauser effect (OE), the solid effect (SE), the cross effect (CE) and thermal mixing (TM). The conventional wisdom states that the OE and the nuclear Overhauser effect (NOE) require rapid motion that governs the relaxation of the electron or nuclear spins and are typically observed in conducting solids (metals and low dimensional conductors) and liquids, respectively. In the case of OE DNP using electrons, near on resonance irradiation yields a symmetric absorptive DNP Zeeman field profile centered about the electron paramagnetic resonance (EPR) line. In contrast, the SE, CE and TM do not require dynamic spins and are observed in insulating solids and yield asymmetric Zeeman profiles. The SE dominates with narrow line polarizing agents (PA) and off-resonance irradiation excites the forbidden DNP transitions at $\omega_e \pm \omega_n$. The CE and TM rely on the three spin couplings and yield dispersive field profiles whose shape depends on the details of the EPR spectrum.

In this paper we consider insulating solids immersed in a strong magnetic field and doped with a PA whose EPR linewidth, $\Delta\omega_{0S}/2\pi$, is much narrower than the nuclear magnetic resonance (NMR) Larmor frequency, $\omega_{0I}/2\pi$. In this

[1] Corresponding author: rgg@mit.edu

case, the CE is attenuated because it requires pairs of electron spins, such that their EPR Larmor frequencies, $\omega_{0S}/2\pi$ differ by the NMR frequency. Furthermore, TM is present when the EPR spectrum is strongly homogeneously broadened, for example, when the PA is small, so the interaction between pairs is large, and the nuclear Larmor frequency low. Finally, when the zero quantum (ZQ) and double quantum (DQ) cross relaxation rates are different, the Overhauser effect yields a symmetric Zeeman profile centered about the electron Larmor frequency [23-27].

However, about a decade ago [2, 28, 29] and more recently in high field DNP experiments using trityl radicals, a dispersive DNP field profile was observed, [30-32], which is difficult to explain as TM. We believe this is because the trityl molecules are bulky, and the interaction between pairs cannot be much larger than about 50 MHz [33, 34]. Furthermore, in the Supporting Information (SI) we calculate the dipole sum for the case that generates the maximum possible electron spin frequency shift in a cluster and the electron frequency shift should be well below 600 MHz where we have performed experiments.

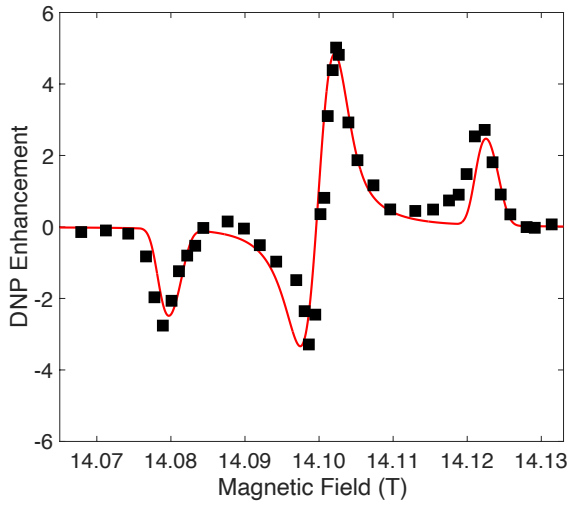


FIG. 1: DNP field profile for a 80mM Trityl-OX063 in $d_6$DMSO:$D_2O$:$H_2O$ (6:3:1) sample at $\omega_{0I}/2\pi$ = 600MHz, 95K with a 8 kHz spinning rate, irradiated with a gyrotron. The solid line is the SpinEvolution simulation using the following parameters: $\omega_1/2\pi$ = 1.6MHz, $T_{1e}$ = 1ms, $T_{2e}$ = 0.2$\mu$s and the cross relaxation times $T_{1ZQ}$ =0.99975 ms, $T_{1DQ}$ = 1ms, $T_{2ZQ}$ = $T_{2DQ}$ = 0.2$\mu$s.

In addition, Karabanov, et al. [32] observed a well-resolved dispersive signal near the EPR center with a trityl concentration of only 15 mM. This low concentration further suggests that it is not TM and probably is an effect involving a single electron spin interacting with surrounding nuclear spins. Furthermore, the experiments were performed under experimental conditions where the OE, the SE, and the CE cannot provide such enhancement.

Finally, in a recent paper[35], we show that even with aggregation of the trityl radicals the electron-electron interaction is not strong enough to induce triple spin flip for

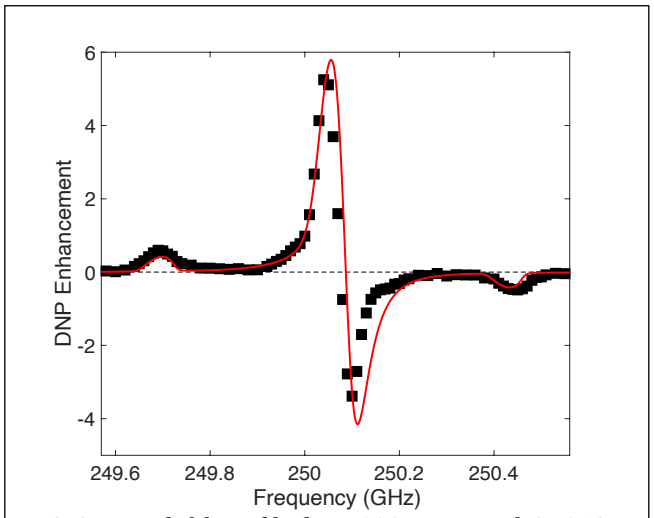


FIG. 2: DNP field profile for a 100 mM Trityl-OX063 in $d_6$-DMSO:$D_2O$:$H_2O$ (6:3:1) sample at $\omega_{0I}/2\pi$ = 380 MHz, 100 K with a 6 kHz spinning rate, irradiated by a 160 mW solid state source. The solid line is the SpinEvolution simulation using the following parameters: $\omega_1/2\pi$ = 0.25 MHz, $T_{1e}$ = 4 ms, $T_{2e}$ = 0.05 $\mu$s and the cross relaxations $T_{1ZQ}$ = 1.9995 ms, $T_{1DQ}$ = 2 ms, $T_{2ZQ}$ = $T_{2DQ}$ = 0.05 $\mu$s.

TM and the spin temperature of the $^{13}C$ is completely decoupled from $^{1}H$. The spin temperatures of $^{13}C$ and $^{1}H$ can even have different signs with microwave irradiation. This proves that the electron-electron coupling is not strong enough to span the nuclear Larmor frequency of $^{1}H$ at 380 MHz so that $^{1}H$ and $^{13}C$ can reside in the same electron spin bath.

In this paper we propose a new mechanism, termed resonant mixing (RM) that explains this dispersive DNP field profile. We first present experimental results illustrating the effect, and then outline the basic principles of this mechanism. We show that it yields a dispersive Zeeman field profile similar to TM.

In order to verify our theory, we recorded the $^{1}H$ DNP Zeeman field profile of a 80mM Trityl-OX063 in $d_6$-DMSO:$D_2O$:$H_2O$ (6:3:1) sample at $\omega_r/2\pi$ = 8 kHz and $\omega_{0I}/2\pi$ = 600MHz, T=95K using a ~ 17W gyrotron microwave source. The Zeeman field profile is shown in **Figure 1** together with a simulation performed with SpinEvolution[36] software. For simulation, typical $T_{1e}$ and $T_{2e}$ values for samples with such concentration are used. A small difference between the ZQ and DQ cross relaxation values are used in order to fit the slight asymmetry between the positive and negative RM enhancements. If the ZQ and DQ cross relaxations are the same, an antisymmetric RM DNP field profile should be obtained as shown by the dashed line in **Figure 4**. An even larger difference between the two cross relaxations would lead to an Overhauser DNP. We believe that this is presently the highest field where a distinctive RM profile is observed. Furthermore, this high nuclear Larmor frequency, quenches the TM, further confirming our argument that the center DNP field profile is due to RM rather than TM. The details of the

simulation using the SpinEvolution software are provided in the SI. In SpinEvolution, the cross relaxation rates are simply defined as the relaxation of the off-diagonal elements of the density matrix as in the Solomon equations [37]. Furthermore, if the electron-electron coupling were greater than 600MHz to allow TM, then TM would be much stronger at low fields, which is not the case. In addition, in **Figure 2** we show a Zeeman field profile recorded from a sample containing 100mM Trityl-OX063 in $d_6$-DMSO:$D_2O$:$H_2O$ (6:3:1) at $\omega_r/2\pi$= 6 kHz and $\omega_{0I}/2\pi$ = 380 MHz, 95 K. We used a frequency swept ~ 160 mW solid state microwave source, and again observed a moderate enhancement $\mathcal{E}$~ 5 instead of the order of 100 observed at 20 K [38]. This may suggest that the temperature and relaxation play a significant role in achieving large enhancements.

Finally, echo detected EPR spectra were recorded with a 140 GHz EPR spectrometer at 80K for an 80mM sample and compared to results from a lower concentration, 8mM sample, shown in **Figure 3**. We observe a small asymmetry in the lineshape from the $g$-anisotropy, which should contribute about 140GHz $\times \frac{2.0032-2.0026}{2} \sim$ 40MHz line width (the g-tensor value is taken from [39]). The detected line width is 45G ~ 120 MHz for both samples. The extra broadening from 8 to 80mM is ~11 MHz. Thus, the electron-electron dipolar interaction should be below 100 MHz as predicted from the size of trityl radicals. Assuming a homogeneous distribution of radicals in the solvent, we estimate the distance between the electron spins for the 80mM sample to be 2.7 nm, corresponding to an electron-electron dipolar interaction of 8 MHz. This confirms the measured line broadening from 8 to 80mM. Therefore, our EPR study argues against the proposition of thermal mixing, as the EPR line width though broadened by the electron-electron dipolar interaction remains below the nuclear Larmor frequency. Thus, the fundamental triple spin flip processes for thermal mixing are attenuated. In going from 140 GHz to 395 GHz, the $g$-anisotropy of trityl will broaden the EPR line by another ~60 MHz, while the electron-electron dipolar interaction is invariant, further attenuating TM. Additional EPR data at 9 GHz is included in the SI.

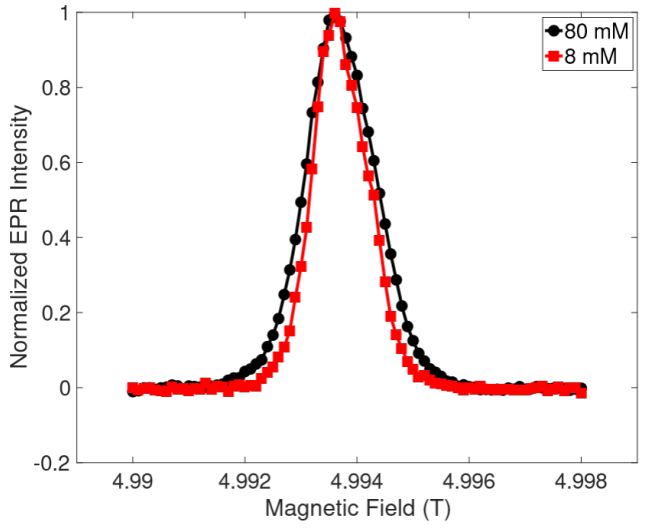


FIG. 3: Echo detected EPR spectra of 8 and 80 mM Trityl in $d_6$-DMSO, $D_2O$ and $H_2O$ (60:30:10) matrix at 140 GHz and 80 K.

In an attempt to understand this dispersive shape of the DNP field profile, we initially performed simulations using SpinEvolution[36]. The results are presented in **Figure 4** for a system consisting of a single $S$ = 1/2 electron spin interacting with a single $I$ = 1/2 nuclear spin. In the absence of relaxation, we observe a weak dispersive DNP enhancement at the EPR resonance. As the simulation involves a single electron spin and hence no electron-electron interactions, this enhancement cannot be ascribed to the CE or TM. In addition, there is no cross relaxation, thus it cannot be due to the OE. Finally, this cannot be the SE, which is observed at $\omega_{0S} \pm \omega_{0I}$.

To understand its origin, we studied the Hamiltonian of a coupled electron-nuclear spin pair with microwave irradiation, which is essential for DNP. Our calculations reveal a new DNP mechanism, different from the OE, SE, CE and TM, that has previously been overlooked. We term this effect *Resonant Mixing (RM)*, since it originates from state mixing induced by microwave irradiation near the EPR frequency.

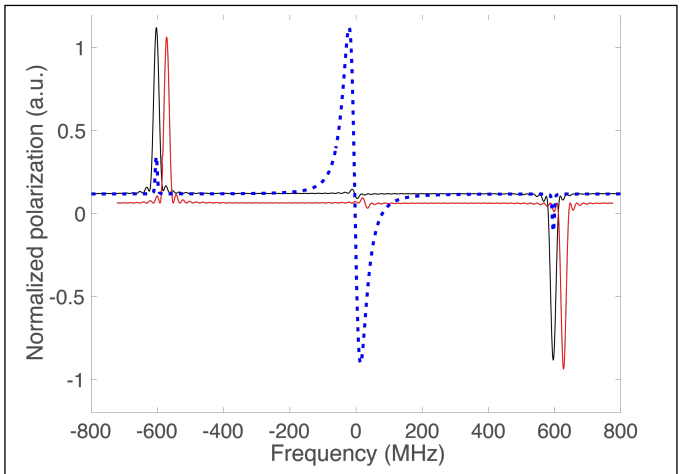


FIG. 4: DNP Zeeman field profile from a SpinEvolution simulation (black) and an analytical calculation using (5) (red) for 1 electron spin interacting with 1 nuclear spin. The red trace is offset from the simulation for clarity. The following parameters are used, $\omega_{0I}/2\pi$ = 600 MHz, $\omega_1/2\pi$ = 0.5 MHz at $t$ = 50 ns (in the order of the spin coherence time $T_{2S}$, see (17)). The dotted line (blue) shows the SpinEvolution simulation in the case of CW irradiation using the following relaxation times: $T_{1e}$ = 1 ms, $T_{2e}$ = 0.2 $\mu$s and the cross relaxations $T_{1ZQ}$ = $T_{1DQ}$ = 1 ms, $T_{2ZQ}$ = $T_{2DQ}$ = 0.2 $\mu$s.

We start by following the treatment for coherent DNP described in [21, 34, 40]. We consider a system consisting of a single $S$ = 1/2 electron spin interacting with a single I=1/2 nuclear spin in the presence of a static magnetic and a microwave field. Per usual, we choose the $z$-axis of the laboratory frame of reference along the static magnetic field and the $x$-axis along the microwave field. In a frame rotating

with the microwave frequency $\omega_m$ about the $z$-axis and with $\hbar = 1$ the truncated spin Hamiltonian is then

$$\begin{aligned}\mathcal{H} &= (\omega_{0S} - \omega_m)S_z + \omega_{1S}S_x - \omega_{0I}I_z \\ &+ S_z A_{zz} I_z + \tfrac{1}{2}S_z\left(A_{z-}I_+ + A_{z+}I_-\right).\end{aligned} \quad (1)$$

The first two terms represent the Zeeman and microwave Hamiltonians of the electron spin in the rotating frame, where $\omega_{0S} - \omega_m$ is the electron resonance offset term and $\omega_{1S}$ the electron Rabi frequency. The next term is the nuclear Zeeman interaction, where $\omega_{0I}$ is the nuclear Larmor frequency. Finally, the last term is the part of the dipolar interaction between the electron and nuclear spin, where $I_\pm = I_x \pm iI_y$. As in the description of nuclear orientation via electron spin locking (NOVEL) and the integrated solid effect (ISE) we neglect the $S_zA_{zz}I_z$ term in the dipolar interaction[41-43].

Our aim is to determine the evolution of the nuclear polarization, $P_I(t)$

$$P_I(t) = \frac{1}{I}\frac{Tr\{\rho(t)I_z\}}{Tr\{\rho(t)\}} \quad (2)$$

after switching on the microwave field, and assuming initial conditions $P_I(0) = 0$ and the electron polarization, $P_S(t)$,

$$P_S(t) = -\frac{1}{S}\frac{Tr\{\rho(t)S_z\}}{Tr\{\rho(t)\}} \quad (3)$$

Here $\rho(t)$ is the density matrix.

In the first step we tilt the frame of reference for the electron spin by $\theta$ such that $\tan\theta = \omega_{1S}/(\omega_{0S} - \omega_m)$. Thus the ˜$z$-axis of the tilted rotating frame is aligned along the effective field. Next, we construct the matrix representation of the Hamiltonian using the basis states,

$$|m_{\tilde{S}}, m_I\rangle = |+\tfrac{1}{2}, -\tfrac{1}{2}\rangle, |-\tfrac{1}{2}, -\tfrac{1}{2}\rangle, |+\tfrac{1}{2}, +\tfrac{1}{2}\rangle, |-\tfrac{1}{2}, +\tfrac{1}{2}\rangle$$

of the $\tilde{z}$-component of $\tilde{S}$ in the tilted rotating frame and the $z$-component of $I$ in the laboratory frame:

$$\frac{1}{2}\begin{pmatrix} \omega_{\text{eff}} + \omega_{0I} & 0 & \frac{1}{2}A_{z+}\cos\theta & -\frac{1}{2}A_{z-}\sin\theta \\ 0 & -\omega_{\text{eff}} + \omega_{0I} & -\frac{1}{2}A_{z-}\sin\theta & -\frac{1}{2}A_{z+}\cos\theta \\ \frac{1}{2}A_{z-}\cos\theta & -\frac{1}{2}A_{z+}\sin\theta & \omega_{\text{eff}} - \omega_{0I} & 0 \\ -\frac{1}{2}A_{z+}\sin\theta & -\frac{1}{2}A_{z-}\cos\theta & 0 & -\omega_{\text{eff}} - \omega_{0I} \end{pmatrix} \quad (4)$$

Here $\omega_{\text{eff}} = \sqrt{(\omega_{0S} - \omega_m)^2 + \omega_{1S}^2}$ is the effective resonance frequency of the electron spin in the tilted rotating frame.

Next, we ignore the matrix elements $\frac{1}{2}A_{Z\pm}\cos\theta$ that slightly mix the nuclear spin states, but not the nuclear and electron spin states, so these terms do not contribute to polarization transfer between the two spins (see Supporting Information)[41, 42]. Thus, the matrix representation reduces to two independent 2 × 2 sub-matrices—one corresponding to zero quantum (ZQ) transitions (the central four elements 22, 23, 32 and 33) and one corresponding to double quantum (DQ) transitions (the outer four elements 11, 14, 41 and 44)—allowing us to solve the Liouville-von Neumann equation analytically. The procedure is straightforward, see for instance the treatment of the solid effect in Wenckebach[21] and similarly for NOVEL and ISE[41-43]. The ZQ and DQ transitions give different signs of the polarization transfer. Accordingly, we subtract the contribution of the ZQ and DQ transitions and find

$$\begin{aligned}P_I(t) &= -P_0\cos\theta\sin^2\theta\left|\tfrac{1}{2}A_{z+}\right|^2 \\ &\times\left[\frac{1}{\alpha_-^2}(1-\cos\alpha_- t) - \frac{1}{\alpha_+^2}(1-\cos\alpha_+ t)\right]\end{aligned} \quad (5)$$

for the evolution of the nuclear polarization. Here we define

$$\alpha_\pm = \sqrt{(\omega_{\text{eff}} \pm \omega_{0I})^2 + \left|\tfrac{1}{2}A_{z+}\right|^2\sin^2\theta}. \quad (6)$$

and $P_0$ as the electron polarization.

In the SE and related mechanisms like NOVEL and ISE, the nuclear polarization occurs at $\omega_{\text{eff}} \approx \omega_{0I}$, but here we are interested in the growth of nuclear polarization when $\omega_{\text{eff}} \ll \omega_{0I}$. To explore this limit we rewrite the expression for $P_I(t)$ as

$$\begin{aligned}P_I(t) &= -P_0\cos\theta\sin^2\theta\left|\tfrac{1}{2}A_{z+}\right|^2 \\ &\times\left\{\left[\frac{1}{\alpha_-^2} + \frac{1}{\alpha_+^2}\right]\sin\frac{\alpha_- - \alpha_+}{2}t\sin\frac{\alpha_- + \alpha_+}{2}t\right. \\ &\left. + \left[\frac{1}{\alpha_-^2} - \frac{1}{\alpha_+^2}\right]\left[2 - \cos\frac{\alpha_- - \alpha_+}{2}t\cos\frac{\alpha_- + \alpha_+}{2}t\right]\right\}\end{aligned} \quad (7)$$

In addition to $\omega_{\text{eff}} \ll \omega_{0I}$, we also have $\left|\frac{1}{2}A_{z+}\right| \ll \omega_{0I}$, so we can expand

$$\alpha_\pm^2 = \omega_{0I}^2(1 - x_\pm) \quad (8)$$

where

$$|x_\pm| = \left|\pm 2\frac{\omega_{\text{eff}}}{\omega_{0I}} + \frac{\omega_{eff}^2}{\omega_{0I}^2} + \frac{\sigma^2}{\omega_{0I}^2}\right| \ll 1. \quad (9)$$

Then

$$\begin{aligned}\frac{1}{\alpha_-^2} - \frac{1}{\alpha_+^2} &\approx \frac{4\omega_{eff}}{\omega_{0I}^3} \\ \frac{1}{\alpha_-^2} + \frac{1}{\alpha_+^2} &\approx \frac{2}{\omega_{0I}^2} \\ \alpha_- + \alpha_+ &\approx 2\omega_{0I} \\ \alpha_- - \alpha_+ &\approx -2\omega_{\text{eff}}\end{aligned} \quad (10)$$

and

$$P_I(t) = -P_0 \cos\theta \sin^2\theta \left|\tfrac{1}{2}A_{z+}\right|^2 \times \left\{ \frac{2}{\omega_{0I}^2} \sin\omega_{\text{eff}} t \sin\omega_{0I} t + \frac{4\omega_{\text{eff}}}{\omega_{0I}^3} \left[2 - \cos\omega_{\text{eff}} t \cos\omega_{0I} t\right] \right\} \quad (11)$$

In a real sample the ESR transition is broadened by anisotropy of the $g$-tensor, hyperfine interaction with neighboring nuclear spins and interaction with neighboring electron spins. This implies a distribution in the values of $\omega_{\text{eff}}$ corresponding to the ESR lineshape. After integration over this lineshape the oscillating terms are averaged with a characteristic time similar to the free induction decay (FID) time, $T_{2S}^* = 1/\Delta_{ESR}$ in which $\Delta_{ESR}$ is the ESR linewidth. After averaging the $\cos\omega_{eff}t$ *and* $\sin\omega_{eff}t$ terms in (11) and inserting the definition of $\theta$, we find an enhanced nuclear polarization

$$P_I^\infty = -P_0 \frac{2\left|A_{z+}\right|^2 \omega_{1S}^2}{\omega_{0I}^3} \frac{(\omega_{0S} - \omega_{\text{m}})}{(\omega_{0S} - \omega_{\text{m}})^2 + \omega_{1S}^2} \quad (12)$$

Here we also expand the definitions of $\theta$ and $\omega_{\text{eff}}$. In a completely similar way we find that the component of the electron polarization along the effective field is reduced by an amount

$$\Delta P_S^\infty = -P_0 \frac{\left|A_{z+}\right|^2 \omega_{1S}^2}{\omega_{0I}^2} \frac{(\omega_{0S} - \omega_{\text{m}})}{[(\omega_{0S} - \omega_{\text{m}})^2 + \omega_{1S}^2]^{3/2}}. \quad (13)$$

The final polarization $P_I^\infty$ has the shape of the derivative of a Lorentzian as a function of the microwave frequency, just as the dispersive shape seen in the center of **Figure 4**. It has extrema at $\omega_{0S} - \omega_{\text{m}} = \pm\omega_{1S}$. In these extrema

$$P_I^\infty = \mp P_0 \frac{\left|A_{z+}\right|^2 \omega_{1S}}{\omega_{0I}^3}. \quad (14)$$

It should be noticed that the transfer of polarization to the nuclear spins is almost instantaneous upon switching on the microwave field: a stationary nuclear polarization is achieved coherently in a time of the order $T_{2S}^*$ . It is due to mixing of the electron and nuclear spin states induced by the microwave field, when it is tuned near the resonance frequency of the electron spins. Therefore, we refer to the effect as resonant mixing (RM)**.** It is also a differential effect because the resulting nuclear polarization is the difference between the contributions of ZQ and the DQ matrices. Furthermore, not all electron polarization is transferred to the nuclear spin.

We note that RM differs fundamentally from the SE because it cannot be described as a process evolving slowly in time with a rate that can be calculated with perturbation theory. For this reason it is difficult to compare the effectiveness of RM and the SE directly. For such a comparison we need a non-trivial extension of our model system which includes relaxation processes.

We assume that the electron spin-lattice relaxation time is sufficiently short, so the electron spin polarization is maintained at its thermal equilibrium value $P_0$ at all times. We also assume that the nuclear spin transfers its polarization through flip-flop transitions to its neighboring nuclear spins at a rate of the order of nuclear transverse relaxation rate $T_{2I}^{-1}$ . In this case the nuclear spin can be considered to be polarized according to the rate equation

$$\left(\frac{\partial P_I}{\partial t}\right)_{\text{RM}} = \mp P_0 \frac{\left|A_{z+}\right|^2 \omega_{1S}}{\omega_{0I}^3} \frac{1}{T_{2I}}. \quad (15)$$

This expression enables us to compare the rate of RM with the rate of the well-resolved SE. Here we ignore any inhomogeneous broadening of the ESR line, but we add transverse relaxation of the electron spin with a time constant $T_{2S}$. Then [21],

$$\left(\frac{\partial P_I}{\partial t}\right)_{\text{SE}} = \mp \frac{1}{8} P_0 \frac{\left|A_{z+}\right|^2 \omega_{1S}^2}{\omega_{0I}^2} h(\omega_{0S} - \omega_{\text{m}} \pm \omega_{0I}). \quad (16)$$

Here $h(\omega)$ is a Lorentzian with a width $T_{2S}^{-1}$ and extrema at $\omega_{0S} - \omega_{\text{m}} = \mp\omega_{0I}$. At these limits

$$\left(\frac{\partial P_I}{\partial t}\right)_{\text{SE}} = \mp \tfrac{1}{8} P_0 \frac{\left|A_{z+}\right|^2 \omega_{1S}^2 T_{2S}}{\omega_{0I}^2}. \quad (17)$$

Thus, we find that RM is slower than the SE by a factor

$$\left(\frac{\partial P_I}{\partial t}\right)_{RM} \Big/ \left(\frac{\partial P_I}{\partial t}\right)_{SE} = \frac{8}{\omega_{0I}\omega_{1S}T_{2I}T_{2S}} \quad (18)$$

Using some typical values for samples used for DNP: $T_{2S}$ = 0.05 $\mu$s, $T_{2I}$ = 2 $\mu$s, $\omega_{0I}/2\pi$ = 400 MHz and $\omega_{1S}/2\pi$ = 0.2 MHz. Then we find for this ratio 1.

In addition, upon comparing (15) and (18), we see that the growth of the SE scales quadratically with $\omega_{1S}$ while linearly for RM. In addition, in a low magnetic field the SE becomes less resolved so the SE and RM will be more difficult to distinguish. Thus, we expect that RM is most easily distinguished from the SE in a high magnetic field using weak microwave irradiation. Additionally, according to (18), a shorter $T_{2S}$ and $T_{2I}$ can lead to a stronger RM/SE ratio. This may potentially explain why RM is more significant with a higher radical concentration [38]. Of course, it is more complicated, as $T_{1S}$ and $T_{1I}$ are also affected by the electron spin concentration.

The red curve in **Figure 4** shows an analytical calculation of the DNP field profile using (5) directly with the same parameters for the SpinEvolution simulation. Note that it reproduces our simulation result. Furthermore, this illustrates that the SE and RM can be calculated from the

same equation (5) derived from the fundamental Hamiltonian (1).

In summary, we propose a new DNP mechanism, Resonant Mixing (RM), that is mediated by state mixing of the microwaves and the hyperfine interaction. It results in a dispersive DNP field profile when microwave irradiation is applied near the EPR resonance, hence the name. The Zeeman field profile is similar to that observed for TM, and we believe RM explains the DNP Zeeman field profile of the some recently published trityl data [35, 38].

The physical origin of RM is a state mixing process induced by the microwave and the hyperfine interaction, similar to the SE. However, SE transitions occur when the microwave field is off-resonance at $\omega_{0S} \pm \omega_{0I}$. In contrast the nuclear polarization in RM is enhanced when the electron and nuclear spin states are mixed when applying an on-resonance microwave field.

We have discussed the transition rates for RM and SE. In the case of CW microwave irradiation, where relaxation has to be considered, the static solution for the Liouville-von Neumann equation balanced by the relaxation is calculated instead of the instantaneous evolution with the Hamiltonian. In this case RM can dominate the field profile as shown by the solid lines in **Figures 1** and **2** as well as the dashed line in **Figure 4** which is a simulation result using the SpinEvolution software. As this paper focuses on understanding the origin of the RM effect, a more sophisticated approach for treating relaxation together with the careful experimental studies of the RM effect will be presented in a forthcoming paper.

Finally, we point out that this is the first proposition and theoretical study of the resonant mixing DNP mechanism. The RM could be an ideal method to enhance MAS NMR to study biomolecules where high magnetic fields are essential for high resolution NMR, and where the microwave power is limited. Karabanov, et al. [32] showed a strong effect with trityl compared to SE and more recently an enhancement of 110 has been observed for by Equbal, et al. [38], illustrating the potential. We believe that understanding the RM mechanism should provide a new path to improve DNP enhancements and expect advances in understanding this mechanism in the future.

## ASSOCIATED CONTENT

**Supporting Information**:

1. X-band CW EPR spectra
2. 600 MHz Zeeman Field Profile
3. Maximum Field in Cluster
4. Contribution of the $A_{z+}\cos\theta$ Term
5. SpinEvolution code

## ACKNOWLEDGEMENT

This work was supported by the National Institutes of Health through grants GM132997 and GM132079 to RGG and the Swiss National Science Foundation through a grant to YQ (No. P500PN 202639). We thank Prof. Songi Han and Asif Equbal for conversations and questions that stimulated these experiments.

## References


(1) Carver, T. R.; Slichter, C. P. Polarization of nuclear spins in metals. *Physical Review* **1953**, *92* (1), 212.

(2) Maly, T.; Debelouchina, G. T.; Bajaj, V. S.; Hu, K. N.; Joo, C. G.; Mak-Jurkauskas, M. L.; Sirigiri, J. R.; van der Wel, P. C.; Herzfeld, J.; Temkin, R. J.; et al. Dynamic nuclear polarization at high magnetic fields. *J Chem Phys* **2008**, *128* (5), 052211. DOI: 10.1063/1.2833582.

(3) Barnes, A. B.; Paepe, G. D.; van der Wel, P. C.; Hu, K. N.; Joo, C. G.; Bajaj, V. S.; Mak-Jurkauskas, M. L.; Sirigiri, J. R.; Herzfeld, J.; Temkin, R. J.; et al. High-Field Dynamic Nuclear Polarization for Solid and Solution Biological NMR. *Appl Magn Reson* **2008**, *34* (3-4), 237-263. DOI: 10.1007/s00723-008-0129-1.

(4) Thurber, K. R.; Tycko, R. Prospects for sub-micron solid state nuclear magnetic resonance imaging with low-temperature dynamic nuclear polarization. *Phys. Chem. Chem. Phys.* **2010**. DOI: 10.1039/c0cp00157k.

(5) Sergeyev, I. V.; Bahri, S.; Day, L. A.; McDermott, A. E. Pf1 bacteriophage hydration by magic angle spinning solid-state NMR. *Journal of Chemical Physics* **2014**, *141* (22). DOI: Artn 22d53310.1063/1.4903230.

(6) Becker-Baldus, J.; Bamann, C.; Saxena, K.; Gustmann, H.; Brown, L. J.; Brown, R. C. D.; Reiter, C.; Bamberg, E.; Wachtveitl, J.; Schwalbe, H.; et al. Enlightening the photoactive site of channelrhodopsin-2 by DNP-enhanced solid-state NMR spectroscopy. *Proceedings of the National Academy of Sciences of the United States of America* **2015**, *112* (32), 9896-9901. DOI: 10.1073/pnas.1507713112.

(7) Sergeyev, I. V.; Itin, B.; Rogawski, R.; Day, L. A.; McDermott, A. E. Efficient assignment and NMR analysis of an intact virus using sequential side-chain correlations and DNP sensitization. *Proceedings of the National Academy of Sciences of the United States of America* **2017**, *114* (20), 5171-5176, Article. DOI: 10.1073/pnas.1701484114.

(8) Ni, Q. Z.; Can, T. V.; Daviso, E.; Belenky, M.; Griffin, R. G.; Herzfeld, J. Primary Transfer Step in the Light-Driven Ion Pump Bacteriorhodopsin: An Irreversible U-Turn Revealed by Dynamic Nuclear Polarization-Enhanced Magic Angle Spinning NMR. *Journal of the American Chemical Society* **2018**, *140* (11), 4085-4091, Article. DOI: 10.1021/jacs.8b00022.

(9) Jaudzems, K.; Polenova, T.; Pintacuda, G.; Oschkinat, H.; Lesage, A. DNP NMR of biomolecular assemblies. *J. Struct. Biol.* **2019**, *206* (1), 90-98, Article. DOI: 10.1016/j.jsb.2018.09.011.

(10) Maciejko, J.; Kaur, J.; Becker-Baldus, J.; Glaubitz, C. Photocycle-dependent conformational changes in the proteorhodopsin cross-protomer Asp-His-Trp triad revealed by DNP-enhanced MAS-NMR. *Proceedings of the National Academy of Sciences of the United States of America* **2019**, *116* (17), 8342-8349. DOI: 10.1073/pnas.1817665116.

(11) Bahri, S.; Silvers, R.; Michael, B.; Jaudzems, K.; Lalli, D.; Casano, G.; Ouari, O.; Lesage, A.; Pintacuda, G.; Linse, S.; et al. 1H detection and dynamic nuclear polarization–enhanced NMR of Aβ1-42 fibrils. *Proc Natl Acad Sci USA* **2022**, *119*, e2114413119. DOI: 10.1073/pnas.2114413119.

(12) Azais, T.; Von Euw, S.; Ajili, W.; Auzoux-Bordenave, S.; Bertani, P.; Gajan, D.; Emsley, L.; Nassif, N.; Lesage, A. Structural description of surfaces and interfaces in biominerals by DNP SENS. *Solid State Nuclear Magnetic Resonance* **2019**, *102*, 2-11. DOI: 10.1016/j.ssnmr.2019.06.0010.

(13) Berruyer, P.; Bjorgvinsdottir, S.; Bertarello, A.; Stevanato, G.; Rao, Y.; Karthikeyan, G.; Casano, G.; Ouari, O.; Lelli, M.; Reiter, C.; et al. Dynamic Nuclear Polarization Enhancement of 200 at 21.15 T Enabled by 65 kHz Magic Angle Spinning. *Journal of Physical Chemistry Letters* **2020**, *11* (19), 8386-8391, Article. DOI: 10.1021/acs.jpclett.0c02493.

(14) Kubicki, D. J.; Stranks, S. D.; Grey, C. P.; Emsley, L. NMR spectroscopy probes microstructure, dynamics and doping of metal halide perovskites. *Nature Reviews Chemistry* **2021**, *5* (9), 624-645. DOI: 10.1038/s41570-021-00309-x.

(15) Ardenkjaer-Larsen, J. H.; Fridlund, B.; Gram, A.; Hansson, G.; Hansson, L.; Lerche, M. H.; Servin, R.; Thaning, M.; Golman, K. Increase in signal-to-noise ratio of > 10,000 times in liquid-state NMR. *Proceedings of the National Academy of Sciences of the United States of America* **2003**, *100* (18), 10158-10163.

(16) Golman, K.; in't Zandt, R.; Lerche, M.; Pehrson, R.; Ardenkjaer-Larsen, J. H. Metabolic imaging by hyperpolarized C-13 magnetic resonance imaging for in vivo tumor diagnosis. *Cancer Research* **2006**, *66* (22), 10855-10860. DOI: Doi 10.1158/0008-5472.Can-06-2564.

(17) Atsarkin, V. A. Dynamic Polarization of Nuclei in Solid Dielectrics. *Soviet Physics Solid State* **1978**, *21*, 725-744.

(18) Abragam, A.; Goldman, M. Principles of dynamic nuclear polarization. *Rep. Prog. Phys.* **1978**, *41*, 395-467.

(19) Abragam, A.; Goldman, M. *Nuclear Magnetism: Order and Disorder*; Clarendon Press, 1982.

(20) Can, T. V.; Ni, Q. Z.; Griffin, R. G. Mechanisms of dynamic nuclear polarization in insulating solids. *J Magn Reson* **2015**, *253*, 23-35. DOI: 10.1016/j.jmr.2015.02.005.

(21) W. T. Wenckebach *Essentials of Dynamic Nuclear Polarization*; Spindrift Publications, 2016.

(22) Niinikoski, T. O. *Introduction to Spin, Magnetic Resonance and Polarization*; 2020.

(23) Haze, O.; Corzilius, B.; Smith, A. A.; Griffin, R. G.; Swager, T. M. Water-soluble narrow-line radicals for dynamic nuclear polarization. *J Am Chem Soc* **2012**, *134* (35), 14287-14290. DOI: 10.1021/ja304918g.

(24) Can, T. V.; Caporini, M. A.; Mentink-Vigier, F.; Corzilius, B.; Walish, J. J.; Rosay, M.; Maas, W. E.; Baldus, M.; Vega, S.; Swager, T. M. Overhauser effects in insulating solids. *The Journal of chemical physics* **2014**, *141* (6), 064202.

(25) Delage-Laurin, L.; Palani, R. S.; Golota, N.; Mardini, M.; Ouyang, Y. F.; Tan, K. O.; Swager, T. M.; Griffin, R. G. Overhauser Dynamic Nuclear Polarization with Selectively Deuterated BDPA Radicals. *Journal of the American Chemical Society* **2021**, *143* (48), 20281-20290. DOI: 10.1021/jacs.1c09406.

(26) Gurinov, A.; Sieland, B.; Kuzhelev, A.; Elgabarty, H.; Kühne, T. D.; Prisner, T.; Paradies, J.; Baldus, M.; Ivanov, K. L.; Pylaeva, S. Mixed-Valence Compounds as Polarizing Agents for Overhauser Dynamic Nuclear Polarization in Solids. *Angewandte Chemie International Edition* **2021**, *60* (28), 15371-15375.

(27) Palani, R. S.; Mardini, M.; Delage-Laurin, L.; Banks, D.; Ouyang, Y.; Bryerton, E.; Kempf, J. G.; Swager, T. M.; Griffin, R. G. Amplified Overhauser DNP with Selective Deuteration: Attenuation of Double-Quantum Cross-Relaxation. *The Journal of Physical Chemistry Letters* **2022**, *14*, 95-100.

(28) Hu, K. N.; Bajaj, V. S.; Rosay, M.; Griffin, R. G. High-frequency dynamic nuclear polarization using mixtures of TEMPO and trityl radicals. *J Chem Phys* **2007**, *126* (4), 044512. DOI: 10.1063/1.2429658.

(29) Hu, K. N.; Debelouchina, G. T.; Smith, A. A.; Griffin, R. G. Quantum mechanical theory of dynamic nuclear polarization in solid dielectrics. *J Chem Phys* **2011**, *134* (12), 125105. DOI: 10.1063/1.3564920.

(30) Corzilius, B.; Smith, A. A.; Griffin, R. G. Solid effect in magic angle spinning dynamic nuclear polarization. *The Journal of chemical physics* **2012**, *137* (5), 054201.

(31) Equbal, A.; Li, Y. X.; Tabassum, T.; Han, S. G. Crossover from a Solid Effect to Thermal Mixing H-1 Dynamic Nuclear Polarization with Trityl-OX063. *Journal of Physical Chemistry Letters* **2020**, *11* (9), 3718-3723. DOI: 10.1021/acs.jpclett.0c00830.

(32) Karabanov, A.; Kwiatkowski, G.; Perotto, C. U.; Wisniewski, D.; McMaster, J.; Lesanovsky, I.; Kockenberger, W. Dynamic nuclear polarisation by thermal mixing: quantum theory and macroscopic simulations. *Physical Chemistry Chemical Physics* **2016**, *18* (43), 30093-30104. DOI: 10.1039/c6cp04345c.

(33) Marin-Montesinos, I.; Paniagua, J. C.; Vilaseca, M.; Urtizberea, A.; Luis, F.; Feliz, M.; Lin, F.; Van Doorslaer, S.; Pons, M. Self-assembled trityl radical capsules - implications for dynamic nuclear polarization. *Physical Chemistry Chemical Physics* **2015**, *17* (8), 5785-5794. DOI: 10.1039/c4cp05225k.

(34) Wenckebach, W. T.; Capozzi, A.; Patel, S.; Ardenkjaer-Larsen, J. H. Direct measurement of the triple spin flip rate in dynamic nuclear polarization. *Journal of Magnetic Resonance* **2021**, *327*. DOI: 10.1016/j.jmr.2021.106982.

(35) Palani, R. S.; Mardini, M.; Quan, Y.; Griffin, R. G. Dynamic Nuclear Polarization with Trityl Radicals. *Journal of Magnetic Resonance* **2023**, *349*, 107411. DOI: 10.1016/j.jmr.2023.107411.

(36) Veshtort, M.; Griffin, R. G. SPINEVOLUTION: a powerful tool for the simulation of solid and liquid state NMR experiments. *J Magn Reson* **2006**, *178* (2), 248-282. DOI: 10.1016/j.jmr.2005.07.018.

(37) Solomon, I. RELAXATION PROCESSES IN A SYSTEM OF 2 SPINS. *Physical Review* **1955**, *99* (2), 559-565. DOI: 10.1103/PhysRev.99.559.

(38) Equbal, A.; Li, Y.; Tabassum, T.; Han, S. Crossover from a solid effect to thermal mixing 1H dynamic nuclear polarization with trityl-OX063. *The Journal of Physical Chemistry Letters* **2020**, *11* (9), 3718-3723.

(39) Lumata, L.; Kovacs, Z.; Sherry, A. D.; Malloy, C.; Hill, S.; van Tol, J.; Yu, L.; Song, L. K.; Merritt, M. E. Electron spin resonance studies of trityl OX063 at a concentration optimal for DNP. *Physical Chemistry Chemical Physics* **2013**, *15* (24), 9800-9807. DOI: 10.1039/c3cp50186h.

(40) Wenckebach, W. T. Dynamic nuclear polarization via the cross effect and thermal mixing: A. The role of triple spin flips. *Journal of Magnetic Resonance* **2019**, *299*, 124-134.

(41) Henstra, A.; Wenckebach, W. T. The theory of nuclear orientation via electron spin locking (NOVEL). *Mol. Phys.* **2008**, *106* (7), 859-871, Article. DOI: 10.1080/00268970801998262.

(42) Henstra, A.; Wenckebach, W. T. Dynamic nuclear polarisation via the integrated solid effect I: theory. *Mol. Phys.* **2014**, *112* (13), 1761-1772, Article. DOI: 10.1080/00268976.2013.861936.

(43) Quan, Y. F.; Steiner, J.; Ouyang, Y. F.; Tan, K. O.; Wenckebach, W. T.; Hautle, P.; Griffin, R. G. Integrated, Stretched, and Adiabatic Solid Effects. *Journal of Physical Chemistry Letters* **2022**, *13* (25), 5751-5757. DOI: 10.1021/acs.jpclett.2c01147.